Estimation of atmospheric boundary layer using Kalman filter technique

Abhik Mukherjee[a,*], Partha Pratim Adhikari[a], P.K. Nandi[a], Pinakpani Pal[b], J. Das[b]

[a] *Computer Science and Technology Department, Bengal Engineering College (DU), PO Botanic Garden, Howrah 711103, India*
[b] *ECSU, Indian Statistical Institute, 203 Barackpore Trunk Road, Kolkata 700108, India*

Received 21 January 2002

Abstract

Sodar provides round-the-clock information about the atmospheric boundary layer (*ABL*). However, computer-based extraction of relevant ABL information from sodar data calls for techniques of image processing to remove the inherent noise. Kalman filter is employed as an alternative methodology to extract the ABL. Thus, it becomes possible to bypass the time-consuming image processing steps, making it faster for real time interpretation of atmospheric conditions from ABL. The technique compares well with the performance of the image processing technique.

Keywords: Kalman filter; Acoustic radar; Boundary layer meteorology

1. Introduction

Sound radar or sodar is a ground-based sensor which sends acoustic wave upwards. The wave gets backscattered from different heights in the lower atmosphere, where the refractive index changes due to inversion of temperature profile. The received signal is recorded by an instrument round the clock, thus generating valuable information about the temperature inversion in the lower atmosphere at different hours. This information forms the basis of Atmospheric Boundary Layer (*ABL*).

Computer-based interpretation of these data involve treatment of these data as an image, with time and height being the two axes and intensity of backscattered signal from a given height at a certain time being plotted along the third axis. A lot of image processing (*IP*) is involved before one can extract the ABL boundary from a given sodar-image. This is mainly due to the different noise sources that contaminate the acoustic wave, a major limitation of sodar [16]. In short, a major part of the time is spent in use of IP techniques to achieve this preprocessing, thus making online interpretation slow and inefficient. Hence, there is a requirement for algorithms with faster time complexity in this domain.

Kalman filter (*KF*) was presented in the year 1960 [11] as an estimation tool. It is a set of mathematical equations that provides a recursive computational solution of the least-squares method [1]. The filter is useful for estimations of past, present, and even future states [22]. KF has been widely used [6] for estimation of meteorological parameters as well as prediction of weather conditions. KF can work better than conventional IP filters for removing noise in atmospheric images.

In the present work, a KF based scheme has been successfully designed to extract the ABL information from sodar data. An overview of KF is presented in Section 2. A review of different techniques of sodar data preprocessing are discussed in Section 2. The scope of applying Kalman filter techniques (*KFT*) in the present scheme are discussed in detail in Section 3. Results and comparative performance with IP based techniques are presented in Section 4 to establish the relevance of the work.

2. Preliminaries

This section is intended to provide the necessary theoretical background before presenting the estimation scheme. The mathematical equations involved in conventional KF is presented. This is followed by a brief survey of the work done in the area of sodar-image processing.

2.1. Kalman filter algorithm

The system is modelled here as a linear, discrete, stochastic sequence described by the following equations:

$$X_{k+1} = \Phi_k X_k + BU + W_k, \quad Z_k = H_k X_k + V_k, \qquad (1)$$

where, X_k is the state vector, Z_k the measurement vector, Φ_k the state transition matrix, H_k the measurement matrix, W_k the process noise vector, V_k the measurement noise vector, B the control sensitivity matrix and U the control vector.

The stochastic disturbance vectors W_k and V_k are treated as zero mean Gaussian noise sequences with the following properties:

$$E[W_i W_j^{\mathrm{T}}] = Q_i \delta_{ij}, \quad E[V_i V_j^{\mathrm{T}}] = R_i \delta_{ij}, \qquad (2)$$

where Q_i and R_i are plant and measurement noise covariances, respectively. The KF equations are given in the following chart:

In this context, K_k is the Kalman gain and $r_k = Z_k - H_k \hat{X}_k(-)$ is called the measurement residual.

2.2. Sodar data preprocessing

The potential of using acoustic sounder system for study of boundary layer in meteorology was pointed out clearly during the early period of its development. Since then attempts have been made to work out a methodology of applying acoustic sounder so as to obtain essential information about the ABL. Most of the early approaches were manual and expert dependent. The experts have to go through the voluminous echogram data before concluding the dynamics of lower atmosphere.

The repetitive nature of patterns on sodar-images become necessary and useful to predict suitable techniques for computer analysis and interpretation. This approach requires a classification scheme for sodar-patterns. Earlier researchers have reported several sodar-pattern classification schemes, e.g. Thomson et al. [19] gave a sodar-pattern classification scheme based on the stability of thermodynamic stratification; Clark et al. [5] have studied the diversity of the sodar-patterns and proposed a numerical classification scheme; Gera [10] indexed the sodar structure with respect to microwave fading; Naiping et al. [15] suggested a few ideas for analysis of the sodar-patterns using statistical characteristics.

Computer techniques have been extensively used for automatic analysis of sodar-patterns since 1980s. Foken et al. [9] have done some pioneering work of classifying various convective and inversion type of sodar-patterns into 2-digit code compatible with computer pattern recognition. According to them, the basic patterns are known to be divided into vertical and horizontal types.

Kalman equations for forecast

Project state ahead	Project error covariance ahead
$\hat{X}_{k+1}(-) = \Phi_k \hat{X}_k(+) + \mathrm{BU}$	$P_{k+1}(-) = \Phi_k P_k(+) \Phi_k^{\mathrm{T}} + Q_k$

Kalman equations for analysis

Compute K_k	Update estimate $\hat{X}_k(+)$	Update covariance $P_k(+)$
$P_k(-) H_k^{\mathrm{T}} (H_k P_k(-) H_k^{\mathrm{T}} + R_k)^{-1}$	$\hat{X}_k(-) + K_k[Z_k - H_k \hat{X}_k(-)]$	$(I - K_k H_k) P_k(-)$

For automatic classification of sodar-pattern Chaudhuri et al. [3,4] have developed some basic concepts. They observed that the shape of the ABL patterns in the sodar-images can be determined from the boundaries. Therefore, a true demarcation line or boundary between the sodar-pattern and the background in the sodar-image needs to be identified. This boundary is an important requirement for recognition of sodar-patterns (and sub-patterns).

The quality of sodar-image and the boundary of sodar-patterns are often degraded and broken due to various man-made and environmental noises and increases the difficulty in interpretation. Standard IP techniques do not seem to remove these noises adequately. Researchers have worked on different pre-processing schemes to enhance the quality of the patterns in the sodar-images [8,20,21]. Unfortunately, such approach is true for specific cases where the presence of noises in sodar-images is marginal. But in practical situations, one cannot guarantee such cases, as sodar-patterns are often degraded in the sodar-images due to noise. Therefore, to minimise the effects of these noises, image pre-processing is required. Pre-processing is very useful in a variety of situations, since it helps to suppress information that is not relevant to specific image processing or analysis task.

Researchers have experimented extensively with the existing techniques for enhancing desired features by using wide variety of sodar-images [7,14]. Various image enhancement algorithms have been suggested for use in sequence with proper tuning suitable specifically for sodar-images [2]. However, the IP based algorithms are generally slow and hence there is a need for faster and more robust scheme for ABL extraction.

3. Design of proposed scheme

In this section, the scheme for ABL extraction from sodar signals based on KF is discussed in detail. The discussion is covered in four parts. The model of different sodar-patterns is covered first. The KF equations involved in the present estimation scheme are presented next. The time and space complexity of the algorithm is analysed for real time estimation of ABL and compared with IP based algorithms. Finally, schemes for tuning the parameters for real time operation are discussed.

3.1. Model of the sodar patterns

Proper application of KF requires a mathematical model of the plant. In the present scheme transition of ABL heights is considered as the plant. Hence, the interest here lies in expressing the consequent height as a function of the currently available heights. The knowledge about ABL patterns is relied upon for this purpose [3].

Sodar-patterns can be divided into two major categories, inversion and plume structures. The gradients of these structures vary both diurnally and seasonally. In case of inversion structures, the height rises in the morning and falls in the afternoon with progress of time with a low gradient. Plume structures occur during the middle of the day and are indicative of high convection in lower atmosphere. The gradient is steep and the height alternates quite frequently. The gradient is steepest at noon. Fig. 1(a) and (b) show typical inversion and plume structures, respectively. Table 1 shows typical values for the slope of sodar-patterns under different conditions.

Now let h_k be the ABL height at the time instant k. The subsequent height h_{k+1} can be expressed in terms of h_k as a change of slope in unit time. The direction of change is decided on the basis of the trend obtained from h_{k-1} and h_k. The state transition model can therefore be expressed as shown in Eq. (3).

$$\begin{aligned} &\text{if} \quad h_k > h_{k-1} \\ &\qquad h_{k+1} = h_k + \tan\theta \\ &\text{else} \\ &\qquad h_{k+1} = h_k - \tan\theta. \end{aligned} \tag{3}$$

3.2. Filter equations in present context

The previous ABL heights are considered to be the basis available for estimating the subsequent ones. With respect to the KF equation (1) and the system model obtained in Eq. (3), the following analogy can be established.

X_k height of ABL as state at time k
Z_k height of ABL as measured at time k

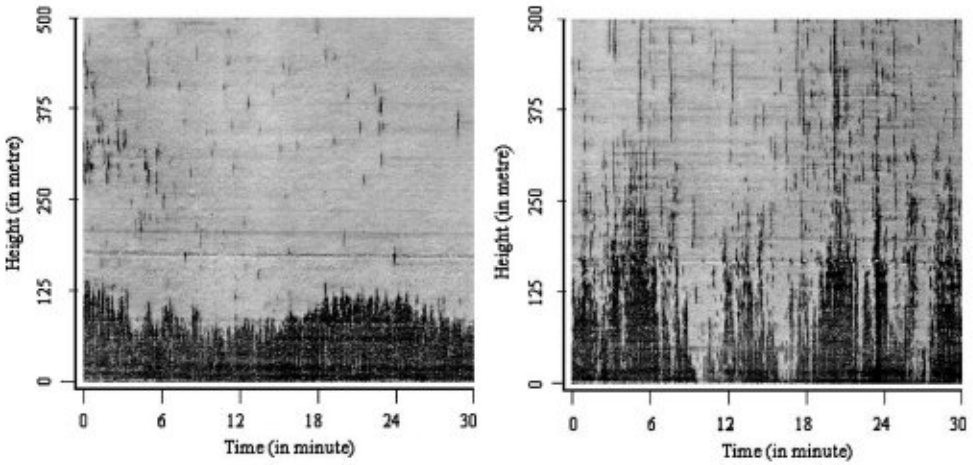

Fig. 1. Two test sodar-images considered for the overall results: (a) inversion, (b) plume.

Table 1
Typical slope (θ) of sodar-patterns in degrees under different conditions

Seasonal condition	Diurnal condition						
	Midnight	Morning	Day	Midday	Afternoon	Evening	Night
Summer	0.0	5.0	30.0	70.0	60.0	30.0	5.0
Rainy	0.0	3.5	20.0	65.0	55.0	20.0	3.5
Autumn	0.0	3.0	25.0	60.0	50.0	15.0	2.5
Winter	0.0	2.0	10.0	50.0	40.0	10.0	2.0
Spring	0.0	2.5	15.0	55.0	55.0	25.0	3.0

Φ_k system model to obtain subsequent height from present state (unity)
U deterministic input ($\tan\theta$)
B unity (± 1)
H_k unity since measured variable and state variable are same
W_k process noise to be augmented to model
V_k measurement noise to be inherent in the system

Hence, the system equations are as follows:

$$X_{k+1} = X_k \pm \tan\theta + W_k, \quad Z_k = X_k + V_k. \tag{4}$$

The process noise W_k arises due to the error inherent in modelling of sodar-patterns. While the actual pattern is very much nonlinear, a linearized version is used here. Details of ABL change are thus missed out. This is considered to be involved in the system equations as process noise, and is assumed to be Gaussian with pre-assigned mean and variance. Deviation from this would have an adverse impact on estimation.

Measurement noise V_k can be attributed to the contamination of acoustic waveform. The received acoustic signal has a time varying Signal to Noise Ratio (SNR). Sodar-image processing involves removal of both multiplicative and additive noise at the image level by using appropriate filters. However in KFT, the ABL height is measured directly. The evolution of ABL being a slow process, the SNR involved with ABL may be assumed to remain constant over time. Hence, any extraneous disturbance affecting ABL height measurement is expected to be additive in nature. KF is capable of removing mainly additive noise and also multiplicative noise to some extent.

The stochastic disturbance vectors W_k and V_k can thus be treated as zero mean Gaussian noise sequences. The reasons for this assumption basically

rely on the fact that the underlying process can be modelled within these constraints. The actual situation is shown while discussing the results.

The KF equations for estimation of ABL heights become:

$$\begin{aligned}
&\hat{X}_{k+1}(-) = \hat{X}_k(+) \pm \tan\theta,\\
&P_{k+1}(-) = P_k(+) + Q_k,\\
&K_k = P_k(-)(P_k(-) + R_k)^{-1},\\
&\hat{X}_k(+) = \hat{X}_k(-) + K_k[Z_k - \hat{X}_k(-)],\\
&P_k(+) = (1 - K_k)P_k(-).
\end{aligned} \tag{5}$$

3.3. Processing time requirements

The overall algorithm works along the following steps:

(1) Convert image to binary form with 1 representing information and 0 background using fixed threshold.
(2) Compute column wise count of 1's as measurement of ABL heights.
(3) Run recursive KF algorithm to estimate ABL heights from measurement.

When real time sodar data are used online as measurement to estimate ABL heights, a globally fixed threshold value is used for measurement. Therefore when a new column is added every six s, [1] it is passed through this global threshold value. The number of 1's in the resulting binary column is considered as the measured ABL height. This is used for estimation by the KF.

Time complexity of steps 1 and 2 of the algorithm would be linear with respect to the row-size (M) of sodar-image for each column and for step 3 it would be O(1) for each column. For estimating the ABL heights for a duration of $6 \times N$ s, the size of sodar-image would be $M \times N$. Therefore, the overall time complexity of this scheme is given by $T_{\text{kft}} = (\text{O}(M) + \text{O}(1)) \times \text{O}(N) = \text{O}(M \times N)$. As regards the space complexity S_{kft}, this scheme would store only the measured ABL height from a single column and storing the data of entire column becomes redundant. Therefore, $S_{\text{kft}} = \text{O}(N)$.

Characteristics of sodar data can be exploited to further reduce the time complexity of the measurement. The intensities in each column can be safely assumed to be sorted. Hence, measurement can be redefined as searching of threshold intensity in the sorted array, which can be achieved in $\lg(M)$ time employing binary search. This mechanism is also capable of rejecting stray high intensities from upper heights. This measurement technique will be referred to as direct thresholding technique (DTT). Hence, $T_{\text{kft}} = \text{O}(N \times \lg M)$.

Conventional IP filters remove noise reasonably well but do not take care of particular structures in sodar-pattern. The method adopted by Chatterjee et al. [2] is a three-step filtering approach specially designed to take into account the subtleties of sodar-images and their characteristic patterns so that a continuous ABL contour can be obtained. This method is referred to as $TSFM$ (three-step filtering method) in subsequent discussion. Since this algorithm provides by far the best results in this domain, complexity and performance of this algorithm is presented for ready comparison with KFT.

TSFM algorithm is performed in three passes:

- *First pass*: This pass tries to remove small gaps between two patches of echo pixels, which may occur due to noise effect. This is done by considering a rectangular neighbourhood of size $m \times n$. If the median value of its neighbourhood is greater than or equal to the current point, then replace its $q \times r$ neighbourhood pixels, where $q < m$ and $r < n$, by the median value.
- *Second pass*: The purpose of this pass is to make thin features more prominent. This is done by applying median filtering using a vertical thin mask (of size $m \times n$, where $m < n$). Thus, discontinuous vertical patterns of significant lengths are joined.
- *Third pass*: In this pass, the same operation as done in the first pass is repeated to fill in any gaps that may still be present.

It is evident that the TSFM algorithm would have to run on moving window technique and an image of size $M \times N$ is required each time. This requires to accumulate few columns (N) before processing. Thus space complexity $S_{\text{tsfm}} = \text{O}(M \times N)$, which is much higher compared to S_{kft}. As regards the time complexity T_{tsfm} of the TSFM algorithm, it is much

[1] An acoustic burst is transmitted upward for a period of 50 ms and the backscattered signal is received over a period of 5.95 s which is the time for sound wave to return back from a height of upto 1 km from the ground base assuming velocity of sound to be about 330 m/s.

higher, since it involves a number of masks designed for filtering. The size of the mask $m \times n$ becomes significant since it is moved around the image. Hence $(M-m) \times (N-n)$ times the mask is moved, each time repeating a computation involving $m \times n$ operations. Assuming p number of such passes, the overall time complexity of the algorithm can be expressed as $T_{\text{tsfm}} = \mathrm{O}(M \times N \times m \times n \times p)$.

In actual implementation, for steps 1 and 3, $m = 5$ and $n = 5$ and for step 2, $m = 1$ and $n = 21$ have been used. Hence, $T_{\text{tsfm}} = \mathrm{O}(71 \times M \times N)$ using m, n as specified. Thus, a significant reduction of processing time is achieved by using the KFT instead of the TSFM. Considering a typical half an hour data with 4 m resolution, $M = 256, N = 300$, and hence $T_{\text{kft}} : T_{\text{tsfm}} = 1 : 2272$. This leaves ample time for employing intelligent pattern recognition algorithms to detect sodar-patterns [13,18] which makes online interpretation feasible.

3.4. Adaptive parameter tuning

Successful application of the scheme in case of real time sodar data would require proper tuning for adapting the parameters to real time conditions of acoustic noise and physical non-linearities.

The measurement is dependent on the choice of proper threshold value. Threshold is chosen on the basis of the work of Otsu [17]. A fixed threshold value of 183 has been used after considering a considerable number of sodar-images. Use of variable threshold would involve computation and hence add to the time complexity of measurement. Errors due to wrong threshold selection has been countered through tuning of measurement noise covariance.

The state transition model discussed in Section 3.1 is fine to model weak nonlinearities. However physical phenomena are strongly nonlinear and hence difficult to model. Table 1 presents only a set of typical values for the slopes to be used for state transition. However there is continuous spatio-temporal variation of the model. The formation of sodar pattern is governed by heat budget of the region that involves complex physical processes like temperature, pressure, wind speed and other dynamic factors as well as static factors like terrain, nature of soil etc. Information regarding the heat budget in the concerned region can be used to change the model slopes dynamically. This results in a piecewise linear model (rather than the linear one) and works better.

In real time there can be large fluctuations of measurement noise statistics. The mean, assumed to be zero, can shift due to measurement bias. Noise covariance can fluctuate due to higher noise levels during daytime, high precipitation during storm and rain, effects of passing vehicles, etc. The values used here are chosen through trial and error over a considerable number of sodar images. The noise cleaning may be improved further by using analytical model of adaptive Kalman filter which can tune the mean and variance of process and measurement noise with time. However since analytical models of noise are unavailable here, heuristics based techniques are suitable for adapting the noise statistics. Measurement residuals are readily available and can be used to make the KF design adaptive using a fuzzy logic based scheme [12].

4. Comparative performance results

The KFT scheme has been described along with its advantages of time and space complexity in the previous section. But it clearly depends on a favourable comparison between the two techniques to show to what extent the KFT can replace the TSFM. For this a set of sodar-images consisting of different sodar-patterns occurring in different seasons at different times of day have been considered. Results for two test images, an inversion (Fig. 1(a)) and a plume (Fig. 1(b)) are reported. Results given in this section are indeed favourable.

4.1. Noise rejection by Kalman filter

A measurement simulation is performed to demonstrate the power of KF in cleaning Gaussian noise with zero mean. ABL obtained by TSFM is deliberately corrupted by noise and used as measurement for KF. Common noise types include zero mean Gaussian, random bias and random walk. Random bias and random walk are correlated and coloured noise. The estimation of ABL heights by KF based on this measurement is found to reject the disturbance to a great extent. Results for the test images Figs. 1(a) and (b) are shown in Figs. 2(a) and (b), respectively.

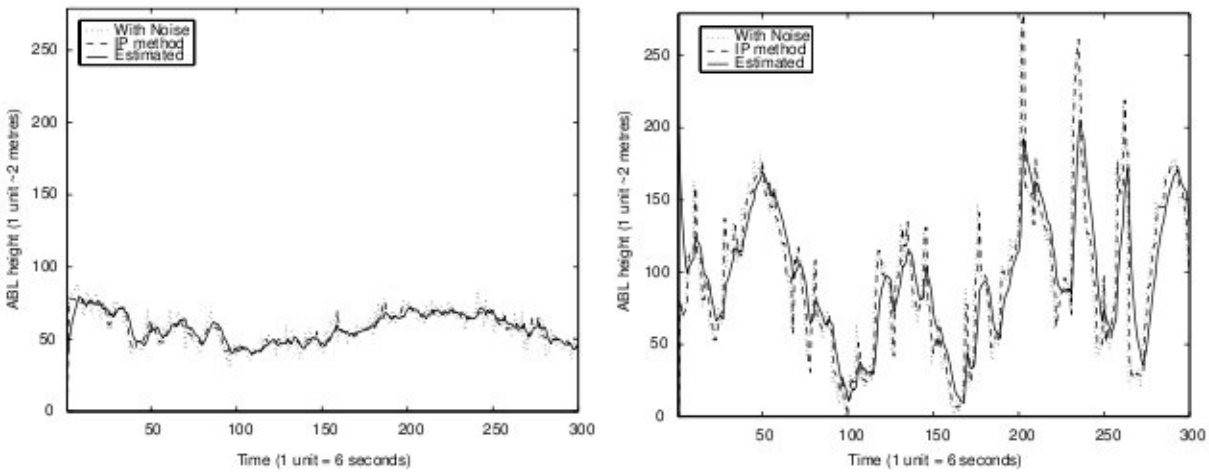

Fig. 2. Estimation by conventional Kalman filter rejects Gaussian noise.

4.2. Nature of measurement error

The ABL heights as measured by the DTT is compared with the ABL heights obtained using TSFM. The error in height measurement can be approximated to Gaussian distribution. The histogram of the relative difference in ABL height for Figs. 1(a) and (b) are shown in Figs. 3(a) and (b), respectively. This result indicates that KFT has a great prospect in ABL estimation since it rejects such disturbance as shown in previous section.

The receiver of sodar signal has to accommodate the entire range of lower atmosphere. Hence, an additional bias is incorporated in the receiver for avoiding the dead zone at lower heights. Hence, the measurement of ABL in KFT has a constant bias of 10–15 m which is absent in TSFM since the mask design removes this bias. This is tackled while obtaining the (nearly) zero means in the histograms shown in Figs. 3(a) and (b), respectively.

4.3. Estimation of ABL height

The actual estimation is performed on the set of sodar-images. The ABL heights as measured by DTT, the ones estimated using KFT and the ones obtained through TSFM are all shown in the same figure for ready comparison. Such results for Figs. 1(a) and (b) are shown in Figs. 4(a) and (b), respectively. The concern here is the difference between the estimated ABL heights and the ABL heights obtained through TSFM. It can be seen that the difference is nominal. In fact, the relative differences have a very small mean and standard deviation. ABL formation is a slow process and the sudden spikes as reported by the TSFM is undesired. Hence, their removal by KFT is favourable.

4.4. Discussions

Some statistics are provided in Table 2 regarding relative difference in ABL heights among the methods for different sodar-patterns occurring in various seasons. It can be seen that inversion structures give more consistent results than plumes. Being a convective process, plumes depict a more turbulent lower atmosphere. The ABL heights not only fluctuate, but also reach much larger heights than in inversion. Hence, the relative difference with respect to the TSFM is higher. However, the evolution of ABL being a slow process, this does not necessarily mean that the KFT result is bad. In fact the estimated value is more likely to be nearer the "true" value, though no exact truth can be sought.

The noise learning capability of KF has been exploited to estimate ABL height. It is worth mentioning that IP techniques in a sense carry out smoothening operation, whereas KF rejects the noise on the basis

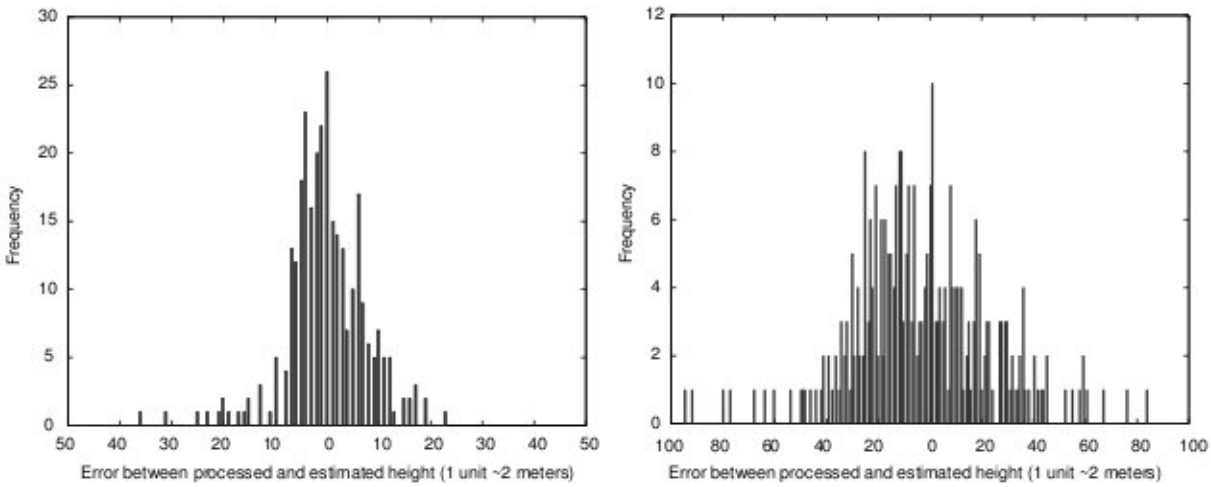

Fig. 3. Error between measured heights and those obtained after TSFM follows Gaussian distribution: (a) the inversion, (b) the plume.

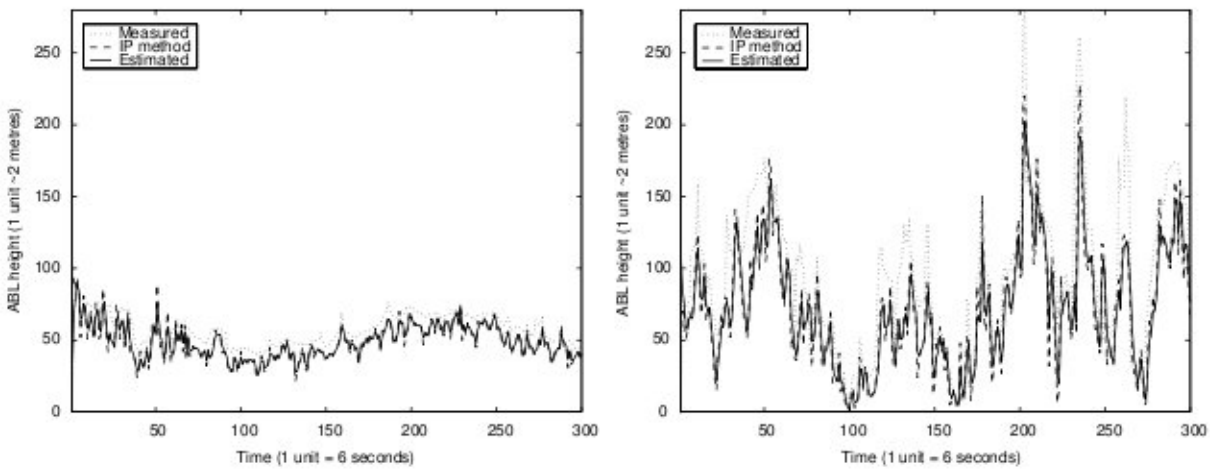

Fig. 4. Heights estimated using KFT along with the heights measured using DTT and heights processed through TSFM.

Table 2
Comparative statistics of the ABL extraction techniques for different type of sodar-patterns

Sodar pattern	DTT–KFT		DTT–TSFM		TSFM–KFT	
	Mean	SD	Mean	SD	Mean	SD
Inversion	6.6183	15.3551	6.6858	17.2400	0.0675	5.2555
Bulge, depression	10.3047	6.0814	10.2667	8.1449	−0.0380	3.8948
Plume, wave	20.1526	19.1699	20.3683	19.9173	0.2157	8.0911

of the approximately available system model. Thus it is more suitable in case of atmospheric images.

5. Conclusion

The framework for designing a Kalman filter based estimation of ABL has been discussed in this paper. Analytical arguments are presented for justifying the use of Kalman filtering technique as an alternative to image processing filters in atmospheric images. Success of the scheme therefore results in computationally faster and robust scheme for ABL extraction. Comparative results substantiate the claims.

Acknowledgements

The motivation of the work was derived from a DST project related to computer based sodar data interpretation sponsored by Department of Science and Technology, Government of India.

References

[1] R.G. Brown, P.Y.C. Hwang, Introduction to Random Signals and Applied Kalman Filtering (with Matlab Exercises and Solutions), 3rd Edition, Wiley, New York, 1997.
[2] N. Chatterjee, P. Pal, J. Das, Boundary extraction of sodar images, Signal Processing 62 (3) (1997) 229–235.
[3] B.B. Chaudhuri, A.K. De, A. Ganguly, J. Das, Automatic recognition and interpretation of sodar records, Indian J. Radio Space Phys. 21 (1992) 123–128.
[4] B.B. Chaudhuri, A. Ganguli, A.K. De, J. Das, Algorithm development for the machine recognition of sodar structure, in: S.P. Singal (Ed.), TATA McGraw-Hill Publication, New Delhi, 1990, pp. 155–160.
[5] G.H. Clark, E. Charash, E.O.K. Bendun, Pattern recognition studies in acoustic sounding, J. Appl. Meteorol. 16 (1977) 1365–1368.
[6] R. Daley, The lagged innovation covariance: a performance diagnostic for atmospheric data assimilation Mon. Weather Rev. 120 (1992) 178–196.
[7] A.K. De, D.P. Mukherjee, P. Pal, J. Das, Sodapreter: a novel approach towards automatic sodar data interpretation Int. J. Remote Sensing 19 (15) (1998) 2987–3002.
[8] A.K. De, S. Tripathy, J. Das, On fine structure of dot echoes as observed by acoustic sounder, Int. J. Remote Sensing 15 (11) (1994) 2157–2165.
[9] T. Foken, K.H. Hartman, J. Kedar, W. Kuchler, J. Neisser, F. Vogt, Possibilities of an optimal encoding of sodar information, Z. Meteorol. 35 (1987) 348–354.
[10] B.S. Gera, Sodar echoes and line of sight of microwave propagation, Master's Thesis, Delhi University, Delhi, 1980.
[11] R.E. Kalman, A new approach to linear filtering and prediction problems, Trans. ASME, Ser. D, J. Basic Eng. 82 (March 1960) 34–45.
[12] A. Mukherjee, P. Adhikari, P.K. Nandi, Features identification for fuzzy logic based adaptive Kalman filtering, in: Asian Fuzzy Systems Symposium, Calcutta, India, Springer, Berlin, 2002.
[13] A. Mukherjee, P. Pal, J. Das, Identification of elementary sodar patterns using perceptrons, in: Proceedings of the Fourth International Conference on Advances in Pattern Recognition and Digital Techniques, Calcutta, India, pp. 83–86, Narosa, December 1999.
[14] D.P. Mukherjee, S.K. Tripathy, A. Chanda, A.K. De, P. Pal, J. Das, Mask design for enhancement of atmospheric images, Image Process. Commun. 3 (1–2) (1997) 25–36.
[15] L. Naiping, C. Jingnan, L. Shiming, Z.Y.S. Lirong, Z. Mingyu, The detection of boundary layer structure with sodar in western mountain area of Bejing, in: S.P. Singal (Ed.), Acoustic Remote Sensing, TATA McGraw-Hill Publication, New Delhi, 1990, pp. 345–356.
[16] W.D. Neff, R.L. Coulter, Acoustic remote sensing, in: D.H. Lenshow (Ed.), Probing the Atmospheric Boundary Layer, American Meteorological Society, Boston, 1986, pp. 201–236.
[17] N. Otsu, A threshold selection method from grey-level histograms, IEEE Trans. Systems Man Cybernet. 9 (1) (1979) 62–65.
[18] P. Pal, A. Mukherjee, S. Acharya, J. Das, Continuous detection of atmospheric pattern from sodar signals, Signal Processing 74 (2) (1998) 153–168.
[19] D.W. Thompson, Acdar meteorology the application and interpretation of atmospheric acoustic sounding measurements, in: Proceedings of the Third Symposium on Meteorological Observations and Instrumentation, (Washington DC, USA), American Meteorological Society, Boston, February 1975, pp. 144–150.
[20] S. Tripathi, A.K. De, J. Das, Computer analysis of atmospheric plume structures, Indian J. Radio Space Phys. 21 (1992) 321–328.
[21] S.K. Tripathy, A.K. De, J. Das, A computer algorithm of noise removal in acoustic radar echograms, Indian J. Radio Space Phys. 22 (1993) 301–305.
[22] G. Welch, G. Bishop, An introduction to Kalman filter, Technical Report UNCCH Computer Science Technical Report 95-041, University of North Carolina, Chapel Hill, NC 27599-3175, 1995.